Heliyon 9 (2023) e22879

Contents lists available at ScienceDirect

Heliyon

journal homepage: www.cell.com/heliyon

Deep learning-assisted IoMT framework for cerebral microbleed detection

Zeeshan Ali [a], Sheneela Naz [b], Sadaf Yasmin [c], Maryam Bukhari [c], Mucheol Kim [d,*]

[a] Research and Development Setups, National University of Computer and Emerging Sciences, Islamabad, 44000, Pakistan
[b] Department of Computer Science, COMSATS University Islamabad, Islamabad, 45550, Pakistan
[c] Department of Computer Science, COMSATS University Islamabad, Attock Campus, Attock, 43600, Pakistan
[d] School of Computer Science and Engineering, Chung-Ang University, Seoul, 06974, South Korea

ARTICLE INFO

Keywords:
Cerebral microbleed (CMB) segmentation
Internet of medical things
Computer-aided diagnostic (CAD) systems
Deep learning
UNet

ABSTRACT

The Internet of Things (IoT), big data, and artificial intelligence (AI) are all key technologies that influence the formation and implementation of digital medical services. Building Internet of Medical Things (IoMT) systems that combine advanced sensors with AI-powered insights is critical for intelligent medical systems. This paper presents an IoMT framework for brain magnetic resonance imaging (MRI) analysis to lessen the unavoidable diagnosis and therapy faults that occur in human clinical settings for the accurate detection of cerebral microbleeds (CMBs). The problems in accurate CMB detection include that CMBs are tiny dots 5–10 mm in diameter; they are similar to healthy tissues and are exceedingly difficult to identify, necessitating specialist guidance in remote and underdeveloped medical centers. Secondly, in the existing studies, computer-aided diagnostic (CAD) systems are designed for accurate CMB detection, however, their proposed approaches consist of two stages. Potential candidate CMBs from the complete MRI image are selected in the first stage and then passed to the phase of false-positive reduction. These pre-and post-processing steps make it difficult to build a completely automated CAD system for CMB that can produce results without human intervention. Hence, as a key goal of this work, an end-to-end enhanced UNet-based model for effective CMB detection and segmentation for IoMT devices is proposed. The proposed system requires no pre-processing or post-processing steps for CMB segmentation, and no existing research localizes each CMB pixel from the complete MRI image input. The findings indicate that the suggested method outperforms in detecting CMBs in the presence of contrast variations and similarities with other normal tissues and yields a good dice score of 0.70, an accuracy of 99 %, as well as a false-positive rate of 0.002 %.

1. Introduction

The Internet of Medical Things (IoMT) is a novel method of connecting medical devices as well as associated applications to clinical technology systems utilizing network monitoring tools. More accurately, it may be characterized as the use of the basics, tools, methodologies, as well as ideas along with the internet notably in the domain of medical sciences.

The established IoMT principles play critical roles whenever medical services must be delivered in certain remote places. There is a

* Corresponding author.
E-mail address: mucheol.kim@gmail.com (M. Kim).

https://doi.org/10.1016/j.heliyon.2023.e22879
Received 14 June 2023; Received in revised form 17 November 2023; Accepted 22 November 2023
Available online 25 November 2023

significant alteration in healthcare, medical procedures, as well as services because of the implementation of IoMT principles and techniques [1,2]. The IoMT looks to be the most likely answer for providing treatment services and recommendations to patients via remote places. On the other hand, the security of these IoMT healthcare systems is of greater importance and can be accomplished with the help of blockchain technologies [3]and federated learning concepts [4]. Similarly, deep reinforcement learning methods are used to handle offloading and scheduling issues in the IoMT framework [5]. Considering established outcomes, IoMT provides diagnostics and treatment convenient as well as reliable. On the other hand, Artificial intelligence (AI)-based computer-aided diagnostic (CAD) systems have recently gained researchers' attention [6–10]. The performance of these CAD systems is relatively high, and more sophisticated systems are developed using advanced image processing and machine-learning techniques. However, these CAD systems can suffer from errors in diagnostics for various reasons. A critical aspect of these systems remains supervision by an expert physician to cross-check the results. The number of available experts for most life-threatening diseases is low, making ensuring their availability difficult, especially in remote locations. Internet of Medical Things (IoMT)-based CAD frameworks aim to ensure the availability of healthcare services for patients from remote locations, especially for life-threatening diseases [11–13]. The IoMT, in conjunction with cloud [14] and artificial intelligence-based techniques, is extremely beneficial in terms of giving more convenient treatment options for different diseases [15].

Cerebral microbleeds (CMBs) are tiny foci of severe brain haemorrhages, appearing as small black dots in magnetic resonance imaging (MRI) of approximately 5–10 mm in diameter [16]. These CMBs are usually caused by microvascular disease and may be identified in the brain and cortico-subcortical locations. Detecting CMBs with the human eye is hard due to their tiny size and similar structure to other normal cells" [16–20]. Therefore, the detection of CMBs by physicians is a complex, time-intensive task and may also suffer from inter-observer variance—different physicians and experts may give different opinions about CMBs' location and existence. CMBs can also be induced by traumatic brain injury (TBI), stroke, and Alzheimer's [18]. The number of CMBs present usually determines the possibilities of cognitive impairment and intracerebral hemorrhage (ICH) [21]. The number of patients with the above-mentioned potential diseases related to CMBs is growing every year. Moreover, microbleeds can amplify the clinical consequences of ischemic stroke, traumatic brain damage, and Alzheimer's disease [22]. Hence, their accurate identification is quite important to ensure correct diagnosis and treatment. Advancements in CAD systems have helped improve and accelerate the diagnosis of different diseases [23–26]. Furthermore, rapid developments in deep learning, the Internet of Things (IoT) [24,27,28], and computer vision have improved the performance of these CAD systems. Because the manual detection of CMBs is complex, time-intensive, and includes potential for error, there has been significant research on the development of automated CAD systems for CMB detection in recent years" [16,22,29]. Still, many open research areas remain available in this particular domain due to the problem's nature.

Existing studies in this field are usually grouped into two categories: (1) a two-phase method including CMB candidate selection and classification and (2) end-to-end deep learning models. The first category requires feature extraction, selection, and classifier training for CMB detection [17,30–33]. More precisely, in these methods features are extracted using different methods such as by applying 2D radial symmetry transform, intensity-based features, Radon-based features, and, local shape features. Following, in the next stage, different machine learning classifiers are used including random forest, Support Vector machines, etc. To perform CMB detection. While great sensitivity may be easily reached in the initial stage of such research studies, but the accuracy of stage 2 (i.e. Classification stage) is frequently poor, resulting in numerous false positives. There is a need for manual removal of false positives if, for instance, the machine learning model is designed to perform CMB detection reliant on shape and intensity features [30]. The process of handcrafted feature engineering is one of the major limitations of traditional machine learning models as well as for accurate CMB detection [34]. This is because the shape and intensity changes of CMBs in SWI image modalities make precise detection extremely difficult. Moreover, sometimes, these methods are semi-automated to reduce false positives, usually added as a post-processing step in CAD systems. The most crucial aspect of these systems is to identify and locate CMBs efficiently and accurately. There are many similar objects like CMBs in images, which induce high false-positive rates. The step of post-processing to lessen false positives requires manual intervention and depends on experts.

Following on, the deep learning algorithms are used in the second class of ways to address such issues in CMB detection. The accuracy of object recognition and image classification can be improved by using deep learning algorithms based on convolutional neural networks (CNNs), thus automating the realm of computer vision [35]. CNN-based improved models have also been proposed by different researchers for CMB detection [36–38]. These end-to-end deep learning models that operate without a post-processing step usually also suffer from high false-positive rates. Blood vessels, which have the same look as CMBs, are one of the false positives produced by these deep learning models [39]. Because the intensity and shape variations between CMBs and normal are too significant to be correctly discriminated, better feature learning that improves model discriminability is more important [40]. Moreover, the availability of a large labelled dataset is also an issue in medical imaging-related tasks. Furthermore, another one of the biggest challenges is the class imbalance issue among CMBs and backgrounds due to their magnitude and sparsity. To address this, numerous techniques are designed in which CMBs and non-CMB patches are chosen equally during training and testing conditions [41–43]. In these methods, given a patch, there exist several CMBs, and hence, patch-level accuracy is distinct from lesion-level accuracy. Although, such techniques demonstrated strong patch-level performance but lesion-level accuracy remains more important for acquiring therapeutically useful insights (e.g. location of CMB in MRI). These issues remain challenging and require efficient end-to-end solutions to contend with patch-based techniques and the reduction of false positives without a post-processing step.

In the context of the preceding existing research, which is primarily based on two-stage frameworks, we suggest an effective, improved UNet-based CMB identification and segmentation for IoMT devices. The primary goal of the proposed UNet-based deep learning model is to build a framework that can detect CMB with high sensitivity while reducing false positives. The improved UNet architecture helps classify CMBs and identify their locations to create an improved treatment plan. In addition, the proposed model handles several challenges, i.e. Post-processing steps are usually carried out in a two-stage model for CMB detection. Second, it does

not necessitate a handcrafted feature engineering calculation, which results in lower performance due to the presence of contrast and comparable morphological structures between CMBs and blood vessels. The proposed model is evaluated on a publicly available dataset consisting of 20 subjects. This study achieves excellent results in terms of the dice score, sensitivity, precision, and false-positive rate and beats all current state-of-the-art published research. The following are the key contributions:

- To detect and segment CMBs, a completely automated end-to-end CAD system is proposed, eliminating patch-based approaches and two-stage frameworks, which take more time and are computationally costly.
- An efficient and improved UNet architecture for CMB detection and segmentation is proposed
- The proposed system minimizes the false-positive rate without manual pre-processing or post-processing steps.
- The dice score of 0.70 achieved with the proposed model is relatively good since CMBs are too tiny to detect and have features and structures that are comparable to other healthy brain cells.

The rest of the paper is structured as follows. Section 2 analyses relevant work, Section 3 explains the suggested technique, and Section 4 details the findings, draws conclusions, and discusses future research.

2. Related work

Current CMB-detection methods are split into two major groups: classification- and feature learning-based methods. Classifier learning uses handcrafted feature learning to train and test the images. For instance, Hong and Lu [25] proposed a deep learning-based method using backpropagation and discrete wavelet transform (DWT). The backpropagation deep learning algorithm was used for classification, while DWT was used for feature extraction reduced using principal component analysis (PCA). Ourselin et al. [13] used multiple radial symmetries transforms (RSTs) for CMB candidate selection and 3D patches to extract features. These features were used to train a random forest for classification purposes and achieved 85.7 % sensitivity. Tao and Cloutier [44] used a genetic algorithm to optimize parameter learning for a backpropagation neural network (BPNN) for CMB candidate selection. Van den Heuvel et al. [33] proposed a model to identify CMB in trauma patients. They extracted 12 features from voxels and CMB candidate locations predicted using a random forest. They also used classification to distinguish CMB from non-CMB and blood vessels. Gagnon [45] used a naive Bayes classifier for CMB detection, achieving 76.90 % accuracy. For CMB identification in persons with cerebral autosomal dominant arteriopathy involving subcortical infarcts and leukoencephalopathy (CADASIL), Zhang et al. [38] employed a neural network model. They examined and assessed three activation functions: (ReLU), Logistic Sigmoid, and Leaky ReLU. Leaky ReLU had the highest sensitivity at 93.05 %. Qian [46] used a cat swarm evolutionary algorithm for CMB detection and identification. Ateeq et al. [47] used a strategy to identify and select the most discriminative features and then used different classifiers for CMB classification; they achieved promising CMB identification and classification results. These traditional approaches function well; nevertheless, they suffer from false positives due to differences in contrast variations and comparable morphological features of CMBs with other normal cells, resulting in low performance. Secondly, these methods require a more meaningful and discriminative feature retrieval that helps the underlying model distinguish CMBs and background. However, due to CMBs' small size and other challenges, designing robust and discriminative feature descriptors is a highly difficult task.

To overcome the problems of traditional machine learning methods, the second category involves automated feature learning using deep learning algorithms. This category includes feature learning using a convolutional neural network (CNN). The convolution process in a CNN also reduces the features and uses the sharing of weights. For instance, Chen et al. [39] used a 3D residual model for CMB identification from 3D images. Transfer learning approaches have also been implemented for the problem of CMB detection. Hong et al. [25] proposed an algorithm based on ResNet for CMB identification and classification; they used a transfer learning concept to improve the training process, achieving 97.46 % accuracy and 95.71 % sensitivity. Furthermore, some deep learning approaches are divided into different stages for CMB detection; they use many pre- and post-processing techniques to obtain the required results in CMB detection. Most recent studies on CMB detection use two-stage frameworks. Dou et al. [16] proposed a 3D Convolutional Neural Network to automatically recognize CMBs with a two-stage framework at the screening and discrimination stage. The volumetric data are inputs to the 3D FCN model for obtaining a 3D volume score in the screening stage. Candidate false positives are removed using the discrimination model in the discrimination stage. Their sensitivity rate is 91.45 %, with an average false-positive rate of 5.74. Liu et al. [34] presented a two-stage methodology for detecting CMB. In the first stage, candidates were selected from susceptibility-weighted imaging (SWI) depending on the combined image's 3D rapid radial symmetrical transforms, referred to as the "candidate selection stage." The second stage involved using deep residual networks with SWI and phase images to remove false positives. The false-positive rate was 1.6, and the precision was 7.09 %. Al-masni et al. [48] suggested a two-phase framework that used the You Only Look Once (YOLO) model to detect possible candidates, followed by a 3D discrimination model to discriminate between false positives and CMBs. In their study, the candidate selection model had a false-positive rate of 52.18, and the false-positive reduction model had a false-positive rate of 1.42. The detection of CMBs in stages is also used in traditional machine-learning algorithms. For instance, Dou et al. [49] proposed a three-stage CMB detection process. The first stage is candidate screening depending on the levels of intensity, the following phase is chronological 3D compact features extraction using stacked convolution Independent Subspace Analysis (ISA), and the last stage is a reduction of false positives using an SVMs trained on the ISA's learned features; they achieved 89.44 % sensitivity. Some patch extraction techniques for CMB detection extract different patches from MRI images. Wang et al. [8] proposed a patch extraction-based method using DenseNet-based transfer learning methods to classify CMBs due to its common use in medical research. Using a sliding window method, they generated training and testing samples by extracting patches from MRI scans. Each sample's target class is determined by the center pixel of each patch. If the pixel in the middle corresponds to the CMB class, the entire sample is

labelled as CMBs. This technique has the problem of data imbalance, which is resolved using the cost matrix in this study, achieving 97.7 % accuracy. Lu et al. [23] also proposed deep learning-based methods with patch extraction and optimization algorithms for CMB detection. Their study generated the dataset by a sliding window approach with brain MRIs. The image features are obtained using already trained VGG preceded by training with an extreme learning machine (ELM) using a Gaussian-map bat algorithm (GBA) for recognition; they achieved 90.05 % accuracy and 93.08 % specificity. Lu et al. [50] proposed an eight-layer-deep CNN to classify CMBs by first extracting patches from MRI images. There were more non-CMB patches than CMB patches, resulting in a class imbalance that was corrected using the resampling approach. They attained a classification accuracy of 96.05 % and a specificity of 97.29 %. Piyush Doke [51] proposed Bayesian optimization-based CNNs. The ultimate optimum hyperparameters are determined via optimization techniques. Since the hyperparameters of machine learning algorithms are critical to their performance. The probability model is built using Bayesian optimization, which maps the probability of a value passing from the objective function to the values of the hyper-parameters—also called score. These possibilities help find the optimal hyperparameters and evaluate the objective function; the models achieved 98.21 % accuracy. Furthermore, Hong et al. proposed the classification of CMBs based on fully optimized CNNs [43] and achieved 98.32 % classification accuracy, 99.74 % sensitivity, and 96.89 % specificity. Wang et al. [11] suggested a CNN model in which they use rank-based average pooling, which outperforms average or max pooling. Both max-pooling and average pooling have some loss of information by selecting maximum values, and average pooling downplays the values of higher activations. Both problems can be solved using threshold-based rank pooling in CNNs. Their method achieved 97.18 % classification accuracy and 96.94 % sensitivity. Hong et al. [52] proposed CNNs with the introduction of center loss. The deeply learned features have discriminative power that is increased by this center loss; hence, the performance of the CNNs is relatively high. They achieved 98.869 % sensitivity and 97.681 % accuracy in their CMB detection. Sa-ngiem et al. [53] proposed CMB detection using area of interest-based segmentation (ROI), identifying the area of the CMBs from the images of SWI. This study employed the mechanisms of shape matching to locate CMBs in the brain MRI, achieving 95.45 % accuracy. In this second category, these proposed deep learning model although shows good performance, still, they require a second stage to remove false positive i.e., post-processing stages. Second, the problem with the patch-based method is that each patch may contain multiple CMBs, and model performance is accessed at the patch level; however, in this case, lesion-level performance is ignored, implying that localizing the CMB location in the MRI image will result in more precise CMBs detection systems. Similarly, during CMB candidate generation, there also exists a data imbalance problem i.e., more patches belong to the non-CMB class and few patches belong to the CMB class. Moreover, problems related to noise in imaging modalities can also be addressed using image-denoising algorithms while detecting cerebral microbleeds [54]. Some enhanced versions of different segmentation algorithms for cerebral microbleeds can also be proposed such as 3D-UNet along with region proposal network [55], cascade network with UNet as a baseline for selecting ROI [56], triplanar ensemble detection network (TPE-Det) model [57], etc.

It is observed from the above literature that most work on CMB detection research is concerned with sensitivity and classification. Candidate selection is the process of finding CMBs from MRI images, while false-positive reduction is the process of finding positive examples of CMBs from negative samples for classification. However, there are two critical issues. The first is the high false-positive rate. Second, the classification of images containing CMBs is not sufficient because specific location identification is also required. We designed an improved UNet-based algorithm for efficient CMB classification and localization to address both issues.

3. Methodology

In this section, we explain the step-by-step procedure of the proposed work. A pictorial representation of the proposed work is depicted in Fig. 1.

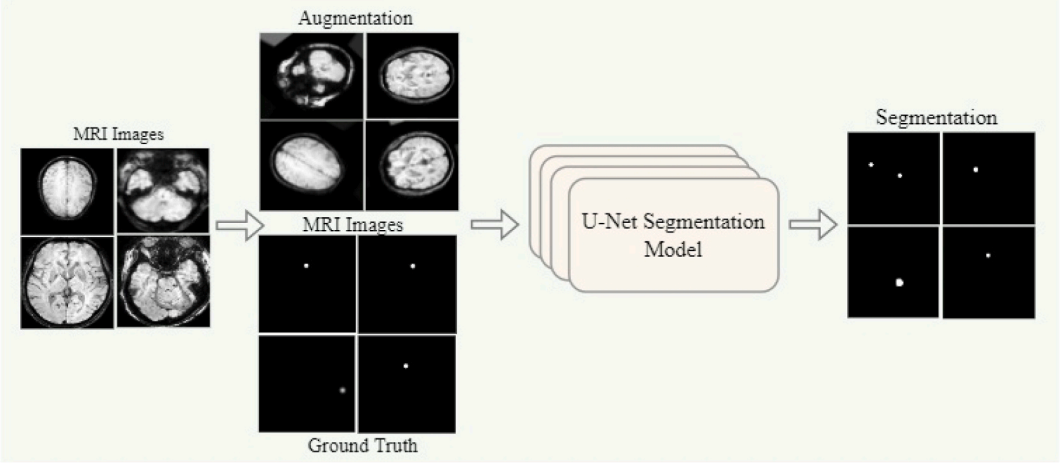

Fig. 1. A proposed methodology for fully automated CMB detection and segmentation.

3.1. Data augmentation

Data augmentation is essential when we have very few training samples to train the network. In the segmentation of bio-medical images, we have very little data and few training samples, which also causes model overfitting. Therefore, excessive data augmentation of different types can increase the training data; it helps the network learn invariance from these different image augmentations.

This study uses different types of augmentation to increase the dataset artificially. One is rotation, in which each image is rotated 10 times randomly at different angles "θ." The other is flipping, in which each image is flipped 10 times randomly on both the horizontal and vertical axes. Rotation is performed with affine transformations that transform an image so that the parallel lines of the image remain parallel afterward. Affine transformations are simple with a transformation matrix. We multiply a point's coordinates with the transformation matrix to obtain the required transformed point, using Equation (1), where M is the transformation matrix:

$$T_p = M * [x\ y1]^t, \text{where 1 facilitates shearing} \tag{1}$$

Image augmentation can be performed by applying different transformations T on an image using Equation (2):

$$A_{image} = T(Image) \tag{2}$$

Where A_{image} is an augmented image after transformation T is applied to image i.e., $T(Image)$. Some samples of dataset are shown in Fig. 2.

3.2. UNet architecture

The UNet architecture used for CMB segmentation was originally developed by Ronneberger et al. in 2015. This model includes a contracting path, an expansive path, and a bottleneck part but with some modifications, including the use of Leaky ReLU, batch normalization, and transposed convolution instead of simple upsampling as in the original UNet. The network architecture with our modification is explained in this section. Fig. 3 illustrates the UNet architecture.

3.2.1. Encoder path

The encoder part is also known as the contracting part and downsampling part of UNet; it comprises four main blocks. Each block comprises two convolution layers of filter size 3 × 3 with the Leaky ReLu activation function and batch normalization preceded by a 2 × 2 operation of max-pooling with stride 2. The use of batch normalization preceded every convolution operation on the down-sampling part increases training speed because the layer's inputs are normalized by using the variance and zero means. As a result, all forward-pass computations are quicker since batch normalization regulates all values flowing into each activation. Moreover, weight initialization is easier when creating deeper networks and produces relatively high overall performance. Therefore, a batch of N different instances in which each instance is a D-dimension vector is given to the batch normalization operation.

The inputs are represented as a matrix, i.e., $X \in R^{N*D}$, where every example is represented by a row xi. Each single example xi is normalized by equation (3):

$$\widehat{xi} = \frac{xi - \mu}{\sqrt{\mu^2 + \epsilon}} \tag{3}$$

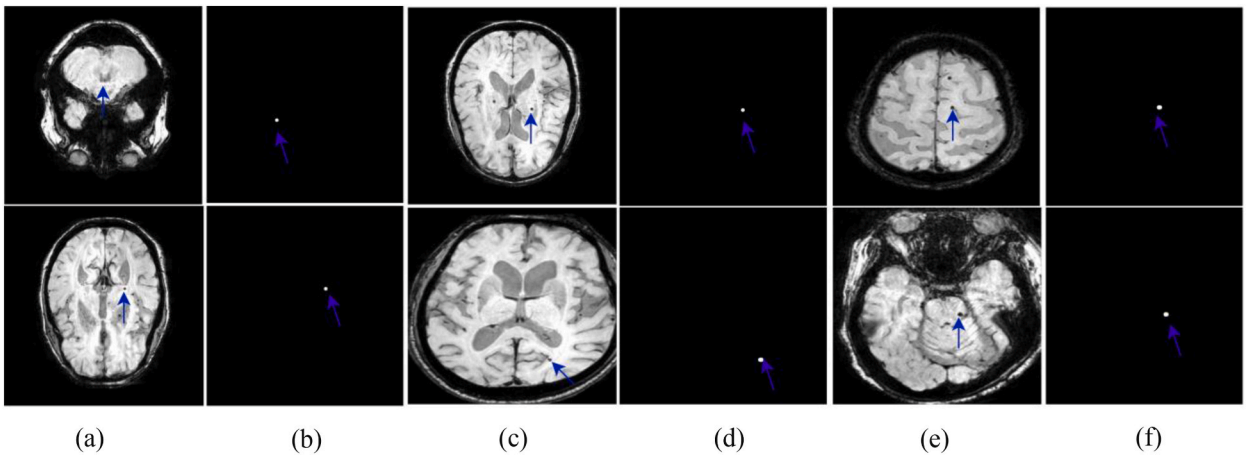

Fig. 2. Different types of images from the CMB dataset and their ground masks with contours around CMBs (a,c,e) shows original images with arrows indicating CMBs and (b,d,e) shows ground truth images with arrows indicating CMBs.

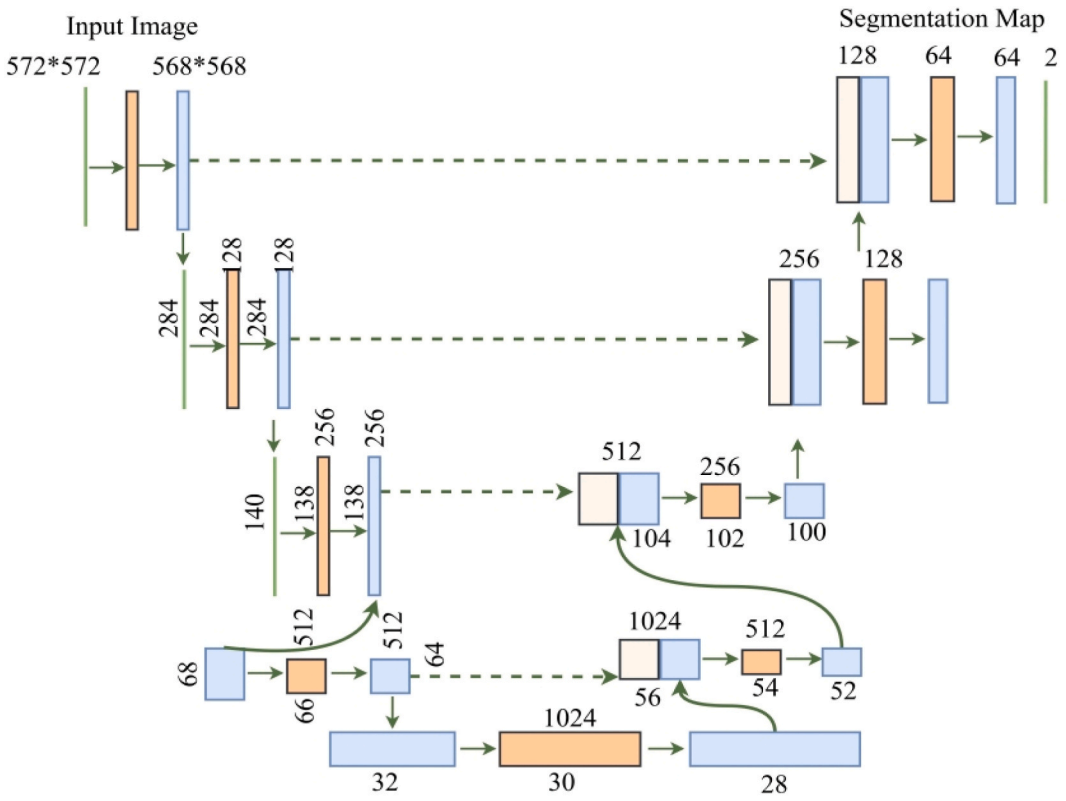

Fig. 3. Improved architecture for UNet used for end-to-end CMB segmentation.

3.2.2. Encoder

where σ^2 is the mean and variance of every input sample in a mini-batch, and ϵ is a constant term that prevents division by zero. The mean and variance formula is give in equation (4):

$$\mu = \frac{1}{N}\sum_i x_i \text{ and } \sigma^2 = \frac{1}{N}\sum_i (x_i - \mu)^2 \tag{4}$$

Then, an affine transform of scale and shift is applied to produce the output of the layer defined by Equation (5), where $\gamma, \beta \epsilon R^{1*D}$ is learned during the training process with original network parameters.

$$y_i = \gamma . \widehat{x_i} + \beta \tag{5}$$

Therefore, the entire layer is expressed by Equation (6), where (dot) is an element-wise product between γ (a row vector) and each row of the matrix $\widehat{X}$.

$$Y = \gamma . \widehat{X} + \beta, \text{ where } \widehat{X} = \frac{X - \mu}{\sqrt{\mu^2 + \epsilon}} \tag{6}$$

Moreover, the activation function "Leaky-ReLU" was used with *alpha*= 0.05 instead of "ReLU." The Leaky ReLU activation handles the dying issue of "ReLU" activation because its slope does not fall to zero. For negative values, it uses a small slope; it also accelerates the training process and creates a more balanced function, as defined by Equation (7):

$$f(X) = \{x \; if \; x > 0 otherwise 0.05x\} \tag{7}$$

A dropout layer of 0.05 is inserted after every max-pooling layer after every convolutional block on the down-sampling path to prevent overfitting by the random deactivation of specific neurons present on hidden layers. The total kernels or filters on the first convolutional operation is 16, doubling for subsequent convolution blocks to 32, 64, and 128 on the last convolution block. The purpose of the encoder path is to draw the features and meanings from an image to describe) the image context most accurately. Up to this path, the model learns and understands what type of information is present in an image with the help of features extracted by downsampling an image using convolution and pooling layers but with a loss of spatial information.

3.2.3. Bottleneck path

The bottleneck part is between the encoder and decoder path. It comprises two convolutional layers with a kernel size of 3× 3 with the Leaky ReLU activation function and batch normalization.

3.2.3.1. Expansive path. The decoder path, also known as the expanding and upsampling path, comprises four blocks. Each block comprises a deconvolution operation with kernel size 3 × 3 and stride 2. Instead of simple up-sampling, a transposed convolution is used as a deconvolution layer. Compared to simple up-sampling, Conv2DTranspose or transposed convolutional are more complex. The transposed convolutions are the inverse of the convolution operation. During the training process, it up-samples images with proper learning to fill in details while a simple up-sampling layer has no weight and only increases the dimensions of the input image. For example, if a convolution specified by kernel w is executed with one stride and no padding, and inputs and outputs are unwrapped into a feature vector spanning left to right, convolution may be expressed as a sparse matrix C, with the non-zero entries $w_{i,j}$ being kernel values. With this matrix, a backward pass can be obtained using the transpose of the C matrix. The loss is amplified by the transpose of C, and errors are transmitted backward. If we multiply a sparse matrix C and the transpose of a sparse matrix C^T, we get a kernel w that specifies a convolution with forward and backward passes. Similarly, A kernel w also specifies a fractionally strided convolution, which computes simultaneously backward and forward rounds through multiplying C and $(C^T)^T$, respectively. After every transposed convolution layer, a concatenation is performed from the encoder path with corresponding feature maps, followed by two convolution layers of filter size 3 × 3 with the Leaky ReLU activation function and batch normalization. The purpose of the decoder path is to up-sample an image to recover and encode the spatial and location details from the feature map size that we lose in the encoder path. With skip connections, all the contextual information from the encoder path is shifted to the decoder path. Skip connections include the concatenation of intermediate outputs of an encoder with input to the intermediate decoder layers at appropriate positions. This concatenation helps combine the localization information of the decoder path with the contextual information of the encoder path.

3.3. Working of proposed model

The architecture of UNet is comprised of three main modules including encoder, bottleneck, and decoder as discussed in the above sections. This section explains the model's step-by-step operation of the proposed model. Hence, more precisely, the first step is to provide a model with a batch of images (MRI and corresponding ground truth) at each iteration. These input images are processed through each part of the UNet. For instance, the encoder module downsamples the images to generate the required set of a feature known as activation maps. These resulting outputs are passed through bottleneck layers and decoder modules. These decoder modules comprised transposed convolution layers that helped us in up-sampling the images to generate the required segmentation maps. Moreover, skip connections among the encoder and decode path are added to fuse the information extracted in both parts of the model. Later on, at the end of the iteration, the loss is computed using actual and predicted segmentation maps, and with the help of the Adam optimizer the weights of the model are updated to be utilized in the next iteration. This process is continued until the model is trained and after training the model weights are saved for testing purposes. All training, hyperparameters, and experimental information are given in the next section 3.4.

3.4. Training details and hyperparameters

Network training is done by searching a CMB dataset for micro-bleed segmentation with an 80:20 split ratio. The CMB images with their annotations were employed to train the network. Training is done with an "Adam" optimizer with a 0.0001 learning rate. An Adam optimizer integrates the momentum term with the stochastic gradient descent and RMSprop; the weight change equation is as follows:

$$W_t = W_{t-1} - \eta \frac{\widehat{m}_t}{\sqrt{\widehat{v}_t + \in}} \tag{8}$$

In the above equation (8), W represents the model weights, η is the step size that depends upon iteration, and $\widehat{m}_t$ and $\widehat{v}_t$ are computed by equation (9), in which β_1 and β_2 are the algorithm's hyperparameters with default values 0.9 and 0.999, respectively.

$$\widehat{m}_t = \frac{m_t}{1-\beta_1^t} \text{ and } \widehat{v}_t = \frac{v_t}{1-\beta_2^t} \tag{9}$$

While training the network, errors or variations between actual and predicted values are measured using the following binary cross-entropy loss function given in equation (10):

$$BCE = \frac{-1}{N} \sum_{i=1}^{N} y_i * \log\left(P(y_i)\right) + (1-y_i) * \log\left(1-p(y_i)\right) \tag{10}$$

Where BCE is the binary cross-entropy, yi is the predicted class of a pixel from model output, and $P(yi)$ is the probability predicted by the model for every pixel being background or foreground. More precisely, classes are formalized as pixels i-e foreground pixels where CMB is present, and background pixels i.e. the area that does not belong to CMBs. The model is trained using BCE loss, which instructs the model on how effectively it classifies the provided MRI image pixels as CMB or non-CMB. Furthermore, a network is trained with

250 epochs with a batch size of 4 and input image dimensions of 256 × 256. Moreover, the implementation is carried out in Python language with Keras and TensorFlow framework, and simulations are run on Google Colab with K80 GPU as well as 12 GB of RAM.

4. Results and discussions

In this section, the outcomes of the suggested model along with evaluation metrics with analysis have been presented. In addition, the details of the dataset as well as the strength and weaknesses of the proposed model is also described:

4.1. Dataset

The dataset employed to check the performance consisted of SWI images collected from 20 individuals for CMB detection and classification; this is the same dataset used in Ref. [16]. Most of the images in this dataset contain more than one CMB. The data samples used in this research were collected from the Philips-medical scheme of 3.0T by setting the iteration to a 17 ms period, 2 mm cut thickness, 1 mm cut separation, in-plane goals of 0.45 × 0.45 mm, 24 ms of reverberation, and 512 × 512 × 150 vol size. An expert rater (Lei Zhao) labelled this dataset, which was then confirmed by a neurologist (Dr. Zhaolu Wang) using the Microbleed Anatomical Rating Scale [29]. The dataset is separated with an 80:20 ratio for training and testing. We performed data augmentation to train the UNet model more accurately. Figs. 4 and 5 illustrate several examples of CMBs and non-CMBs from the dataset.

4.2. Performance evaluation

The proposed study's performance is evaluated on different image segmentation metrics involving the dice score, Jaccard index, asymmetric volumetric difference (SVD), and AUC-ROC. Furthermore, precision, sensitivity, specificity, and accuracy are calculated. The performance evaluation is conducted to verify how close the actual labels are to the predicted labels. The robust image segmentation metrics are the Jaccard index and the Dice score. The Jaccard index is also referred to as the intersection over union (IOU) score; this metric counts the number of pixels in total that are the same among the actual and predicted GT divided by the entire value of pixels that are present in both the actual and predicted mask. In contrast, the overlap between two binary masks is measured using the Dice similarity coefficient. The SVD measures the difference between actual and predicted masks. Sensitivity is the percentage of the True positive values that are actually true. The number of predicted false labels compared with the true-false labels is defined as specificity. These performance measures can be mathematically computed by following equations 11–17:

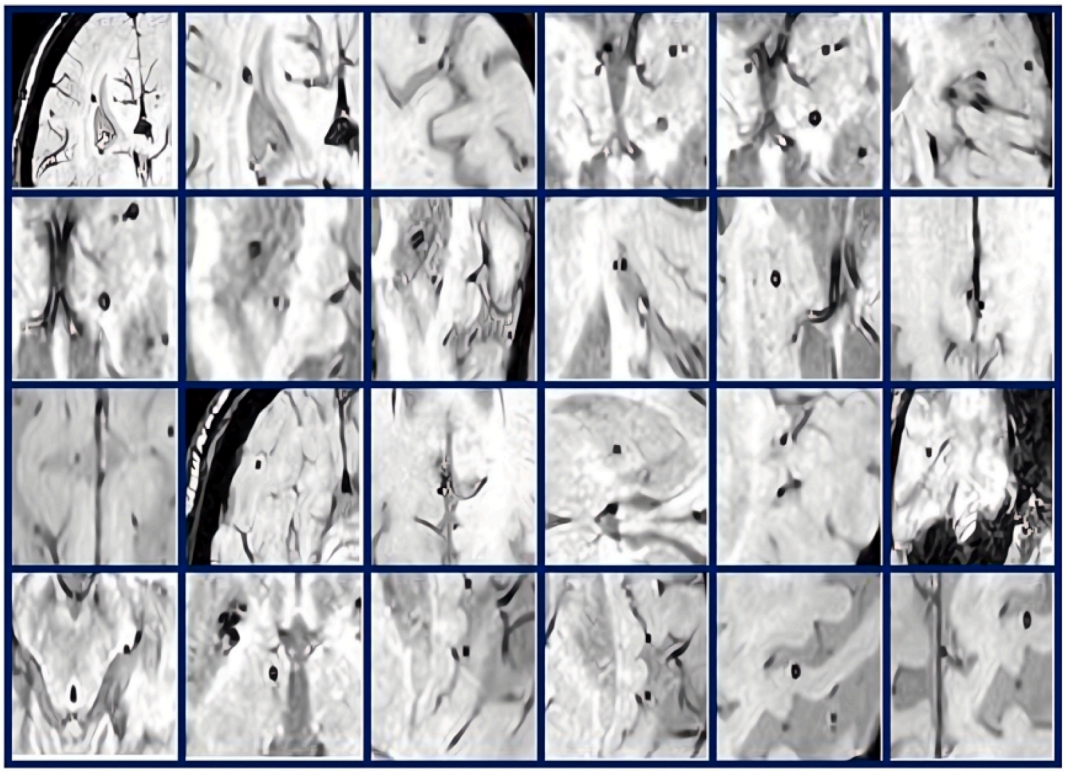

Fig. 4. Samples of non-CMBs in brain MRIs from the CMB dataset.

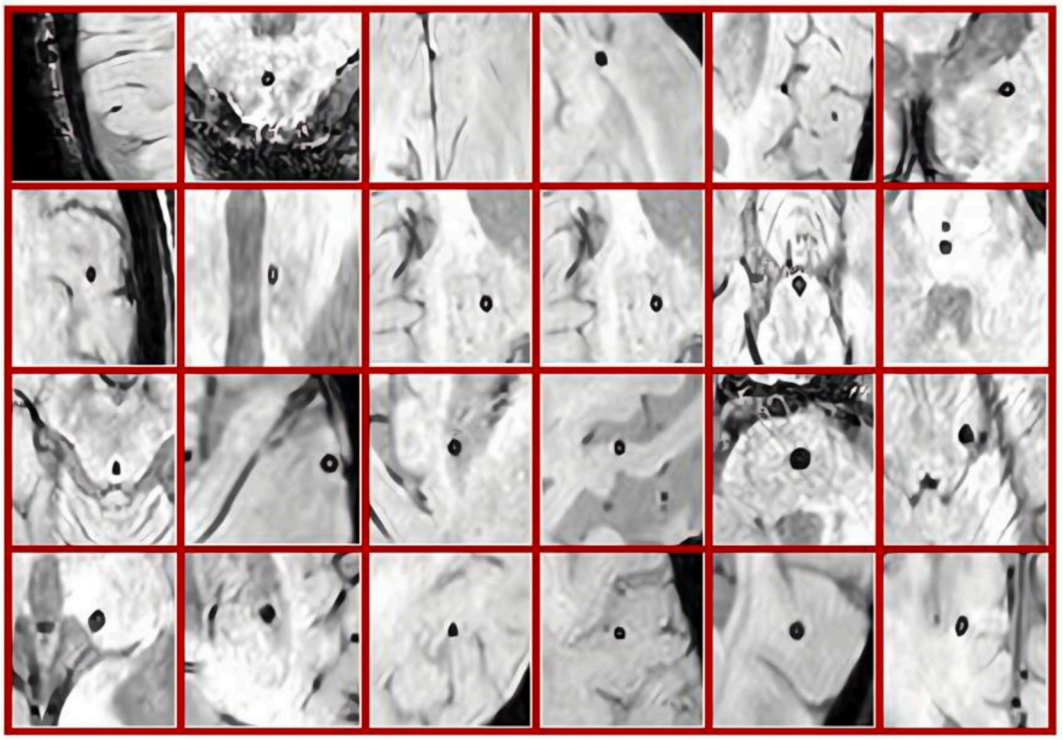

Fig. 5. Samples of CMBs in brain MRIs from the CMB dataset.

$$\text{Accuracy} = (\text{TP} + \text{TN})/(\text{TP} + \text{TN} + \text{FP} + \text{FN}) \tag{11}$$

$$\text{Sensitivity} = (\text{TP})/(\text{TP} + \text{FN}) \tag{12}$$

$$\text{Specificity} = (\text{TN})/(\text{TN} + \text{FP}) \tag{13}$$

$$\text{Precision} = (\text{TP})/(\text{TP} + \text{FP}) \tag{14}$$

$$\text{Dice} = \frac{2\text{TP}}{2\text{TP} + \text{FP} + \text{FN}} \tag{15}$$

$$\text{Jaccard Index} = \frac{\text{TP}}{\text{TP} + \text{FP} + \text{FN}} \tag{16}$$

$$\text{SVD} = 1 - \text{DiceScore} \tag{17}$$

where TP is a true positive, FP is a false positive, TN is a true negative, and FN is a false negative.

4.3. Experiments and discussions

This section summarizes the findings of our improved UNet-based CMB detection and segmentation model. CMB detection remains a challenging task in CAD systems due to its tiny size as well as the existence of CMB mimics including calcifications. The CMB detection system often finds it difficult to detect CMBs due to skull tissues in images. The bone tissue has similar signal properties, and its presence often leads to a high false-positive rate. Therefore, the researchers used a manual brain skull removal procedure that included additional costs and human intervention. This study can directly identify and segment CMBs from complete MRI images without human intervention. Table 1 gives the performance outcomes of the proposed model. The dice score achieved by the proposed

Table 1
Accuracy, Dice score, AUC-ROC, false-positive rate, and Jaccard score results.

Accuracy	Dice Score	AUC-ROC	False-positive Rate	Jaccard Score	SVD	Error (BCE)
99 %	0.70	0.85	0.002 %	0.67	0.3	0.000156

model is 0.70 with 99 % accuracy and BCE (binary cross-entropy) error on the test set in 0.000156, which is relatively good as compared with existing systems. The high accuracy of the proposed IoMT-assisted framework helps new physicians in training and cross-validation. In addition, it also provides confidence to new physicians to improve their judgment.

The most critical aspect of CMB detection and identification is the false-positive rate, often ignored in most research. CMB cells are so similar to other normal brain cells that it is often challenging to distinguish between them. The difficulty differentiating between healthy and CMB cells often leads to ignoring this critical aspect. The proposed system produces excellent performance, with a false-positive rate of 0.002 %. This false-positive rate is the lowest achieved so far, demonstrating the performance of our proposed system. Moreover, from Table 1, it is also observed that the accuracy of the model is high as compared to the dice score. The rationale behind this high accuracy is class misbalance. More precisely, with a given MRI image, the model classifies each pixel as either CMB or non-CMB class, however, due to the small size of the CMB lesion, the number of pixels associated with the CMB class is much less than that non-CMB or background pixels. In this example, even if the model accurately classifies the background pixels as non-CMB and performs poorly on CMB pixels, performance is still great since accuracy does not imply class imbalance. As a result, in this scenario, the dice score is a better assessment measure since it determines the overlap area between the actual and predicted ground truth, and it has been found that a dice score of 0.70 is quite good and indicates that the model identifies the CMB correctly at the lesion level or in terms of location.

Fig. 6 illustrates the results images with CMBs highlighted. More precisely, in Fig. 6, the top row shows the actual MRI images, and the bottom row is the results of the model highlighting CMBs in the form of pixel-level or lesion-level classification. False positives for life-threatening diseases can be critical and should be managed appropriately.

The IoMT-based CAD system ensures the reduction of these false positives, and expert physicians can use this framework when providing their opinion, ultimately reducing the error rate. The other aspect of efficient CAD for CMB detection is the segmentation or localization of the CMB from the image, which would help experts make better decisions. No previous studies have localized or segmented each pixel from the complete MRI image as CMB or non-CMB. The proposed UNet-based efficient method segments out CMBs precisely from the MRI.

The Dice score measures the performance of the UNet-based segmentation, displaying how many pixels match the precise mask or ground truth of the real CMB. We achieved segmentation with a dice score of 0.70, which is pretty high given that CMBs are extremely small, accurately identifying each pixel necessitates a highly precise algorithm, because some other healthy cells have the same structure as the CMB. Furthermore, the Jaccard score is 0.67, as seen in Table 1. CMBs can be an early indicator of intracerebral hemorrhage (ICH) [64] and intracranial hemorrhage (ICH) is the most severe hemorrhage with a significant death risk [65]. Cerebral microbleeds can be a sign as well as a risk factor for future intracerebral hemorrhage [66]. Hence, for their early detection with good performance, an automated CAD system is of greater necessity. The fundamental challenge in developing an effective and dependable CAD system for CMBs is that their size, texture, and structure are comparable to those of other normal tissues. Automating the handling

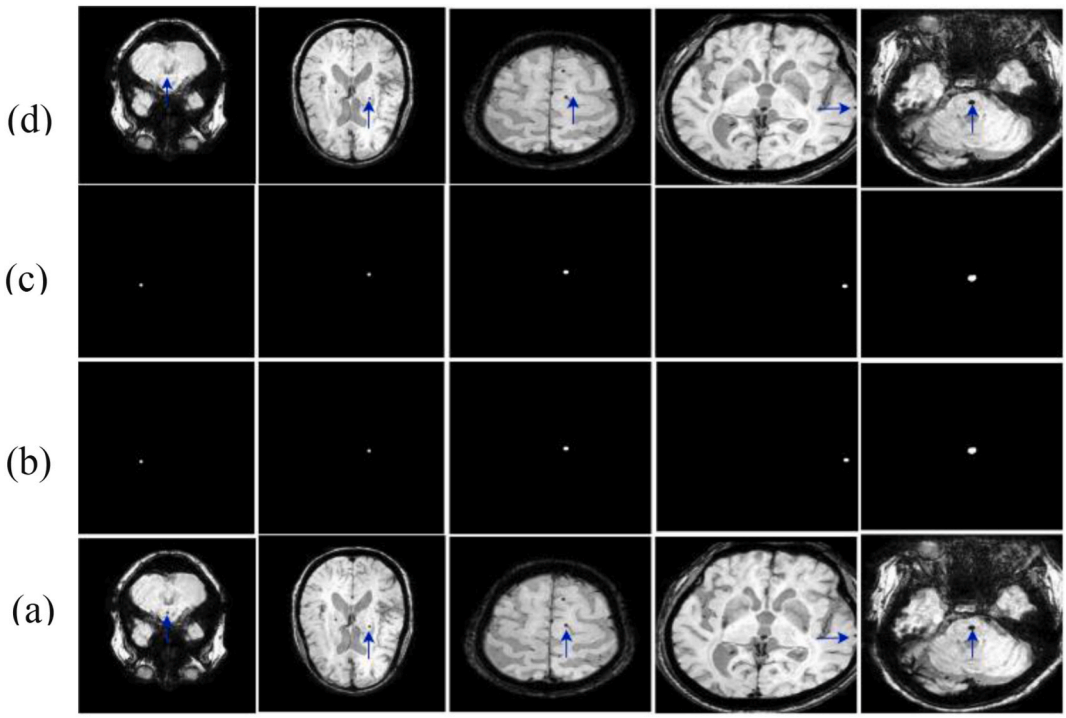

Fig. 6. Results of CMB segmentation from MRI images with their predicted masks (a) shows original images with arrows indicating CMBs (b) shows predicted images (c) shows ground truth images (d) shows predicted images with arrows indicating CMBs.

of these issues is highly desirable, even with a physician's assistance. According to some studies, the clinical practice for annotating CMB is reliant on visual examination as well as manual localization that has low repeatability among various analysts and can be tedious, error-prone, and time-consuming, particularly when large numbers of participants are present" [16,29]. Throughout the CMBs identification procedure, a tradeoff between true positive detection rates (TPR) and the number of false positives (FPs) was identified. As a result, a secondary scanner, whether through another specialist or even by automated computer-aided detection (CAD), is required to improve the effectiveness of microbleeds identification evaluation [22]. To deal, with such challenges, we designed an automated CAD system for the efficient detection of CMBs. The suggested model is compared with different studies, as indicated in Table 2. CMBs are difficult to detect since they are too small and cannot be visible. Contrast variations and similarities with other normal tissues make CMB detection more challenging. More specifically, there are several hard CMB mimics, such as flow voids, calcification, as well as cavernous malformations that approximate the appearances of CMBs in SWI scans thus significantly impeding the identification procedure. In addition, CMBs' widely dispersed locations actually make precise detection much more difficult [16–20]. In the presence of such issues, the proposed method still works well in detecting CMBs from different researchers used different traditional machine learning and deep learning models for CMB detection and identification. Table 3 provides the outcomes in terms of false-positive rates, which demonstrates that our proposed method achieves the lowest false-positive rate among existing research. Furthermore, the suggested method needs no pre- or post-processing stages for CMB detection. Existing work frequently necessitates a pre-processing stage to remove the brain skull and a post-processing stage to reduce false positives. Nonetheless, the proposed approach requires just images with the ground truth and effectively extracts CMBs.

5. Conclusion

Traditional CAD systems have gained popularity in recent years due to advancements in AI and image-processing techniques. These CAD systems lack smart decision-making and analytics capabilities, especially in ubiquitous environments. CMBs can be an early indicator of intracerebral hemorrhage and are very difficult to detect due to their size and similar structure to normal tissues. This factor includes the issue of a high false-positive rate; these systems require pre-processing for brain skull removal and post-processing steps for false-positive reduction. Fully automated IoMT-based CAD for CMBs remains a difficult endeavor that can integrate expert physician feedback. This research focuses on addressing these problems by suggesting an end-to-end UNet-based CMB detection and segmentation that is efficient and entirely automated. The contributions of this article include addressing several challenges in existing computer-aided diagnosis systems for CMB detection. More precisely, the suggested technique, which is based on deep learning, is a one-stage model that operates standalone on a whole MRI image to detect CMBs, as opposed to two-stage alternatives that need post-processing steps. Secondly, it also gives advantages over patch-level methods that suffer from data imbalance problems. It also saves time by manually annotating CMB patches as well as an equivalent amount of non-CMB patches to guarantee class balance during training and testing. Finally, it has advantages over traditional machine learning methods in which the design of robust feature descriptors is critical to detect CMBs in the presence of contrast and morphological differences between CMBs and other normal cells. Moreover, the suggested framework needs no pre- or post-processing steps. The proposed system works without removing the brain skull and requires no human intervention as a post-processing phase to lessen the false positives.

The findings of the study indicate that the suggested technique detects and segments CMBs from brain MRIs effectively. This study produces excellent results in terms of sensitivity and the false-positive rate, at 99 % and 0.002 %, respectively. The practical implications of this research include several advantages, for instance, it can work as an assistance for many clinical applications including research on Alzheimer's, Parkinson's, stroke, hemodialysis, as well as TBI. Since CMBs can be an early indicator of intracerebral hemorrhage (ICH), hence, their early and error-less detection is extremely important using accurate CAD systems. The suggested technique also allows researchers to investigate the relationship between the existence of CMBs and the likelihood of cognitive problems or intracerebral hemorrhage. It assists radiologists in completing their tasks more quickly while manually annotating the CMBs in clinical procedures.

Furthermore, it is vital to describe the limits of the suggested work in order for future researchers to enhance the work. Hence, one possible limitation of this work is the limited data and single dataset. In this single dataset, one kind of acquisition setup, such as 24 ms of reverberation, small cohort, specific field strength, and any other, is used. To more accurately evaluate the performance of the proposed work, more experiments need to be performed on some other large-scale and more diverse CMB datasets. Hence, one potential future research direction is to enhance the generalization ability of the model, i.e. cross dataset training and validation. Moreover, the proposed model works with 2D spatial feature representation and, hence, is limited in utilizing full contextual details of MRI images e.g. 3D volumetric data. Since, in the proposed model, convolution filters are applied directly over the MRI's input slices,

Table 2
Comparison of proposed model with state-of-the-art approaches in terms of accuracy.

Author	Technique	Sensitivity	Accuracy
Lu et al. [23]	Machine Learning SVM	93.0 %	90.0 %
Hong Lu et al. [25]	PCA + Shallow Neural Network	88.47 %	88.3 %
Tao et al. [44]	GA + NN	72.90 %	72.90 %
Wang et al. [58]	CNN	97.22 %	97.35 %
Ateeq et al. [47].	QDA and SVM	93.7 %	97.3 %
Proposed	UNet	99 %	99 %

Table 3
Comparison of proposed model with others in terms of false-positive values per subject and CMB.

Authors	Sensitivity Rate	False-positive value/sub	False-positive value/micro bleed
Ateeq et al. [47]	90.5 %	65.8	6.3
Saghier et al. [59]	50 %	–	–
Bames et al. [12]	81.7 %	107.5	5.4
Ghafryal et al. [60]	90.9 %	4.1	1.8
Bian et al. [61]	86.5 %	44.9	1.5
Dou et al. [49]	89.4 %	7.7	0.9
Chen et al. [39]	89.1 %	6.4	–
Douh et al. [62]	93.16 %	2.74	–
Heuvel et al. [63]	89 %	25.9	0.29
Proposed Method	99 %	0.002	–

therefore, these filters are not shared among the third dimension. Hence, exploiting spatial features from all three dimensions using 3D kernels is critical for our CMB identification framework. Moreover, there may be several CMBs in every slice, therefore making the model capable of counting and localizing CMBs at the instance level per slice is an interesting future endeavour. Any algorithm designed to be used in clinical practice needs to be trained and evaluated not only to recognize CMBs on SWI but also on T2* images as this is a sequence more commonly employed in the clinical setting for CMB detection than SWI. T2* weighted imaging are collected more quickly than SWI (i.e. reduced scan time), which can be useful in clinical practice. In order to test scalability of algorithms, it is necessary to validate their performances on different modalities, since in different test centers different types of sequences are used to diagnose brain related abnormalities. Hence, the applicability of the suggested model across multiple modalities rather than only SWI images is also a promising future direction.

Funding

This research was supported in part by the National Research Foundation of Korea (NRF) grant funded by the Korea government (MSIT) (No. 2021R1A2C109550811) and part by Korea Institute for Advancement of Technology (KIAT) grant funded by the Korea Government (MOTIE) (P0012724, The Competency Development Program for Industry Specialist).

Data availability statement

Data will be made available on request.

CRediT authorship contribution statement

Zeeshan Ali: Writing – review & editing, Writing – original draft, Methodology, Conceptualization. **Sheneela Naz:** Methodology, Investigation, Conceptualization. **Sadaf Yasmin:** Validation, Methodology, Investigation. **Maryam Bukhari:** Validation, Methodology, Investigation, Formal analysis. **Mucheol Kim:** Writing – review & editing, Validation, Project administration, Funding acquisition, Conceptualization.

Declaration of competing interest

The authors declare that they have no known competing financial interests or personal relationships that could have appeared to influence the work reported in this paper.

References

[1] B. Lin, S. Wu, COVID-19 (coronavirus disease 2019): opportunities and challenges for digital health and the internet of medical things in China, OMICS A J. Integr. Biol. 24 (5) (2020) 231–232.
[2] S. Juneja, et al., A perspective roadmap for IoMT-based early detection and care of the neural disorder, dementia, Journal of Healthcare Engineering (2021) 2021.
[3] A. Lakhan, et al., Blockchain multi-objective optimization approach-enabled secure and cost-efficient scheduling for the Internet of Medical Things (IoMT) in fog-cloud system, Soft Comput. (2022) 1–14.
[4] A. Lakhan, et al., Federated-learning based privacy preservation and fraud-enabled blockchain IoMT system for healthcare, IEEE J. Biomed. Health Inf. 27 (2) (Feb. 2023) 664–672, https://doi.org/10.1109/JBHI.2022.3165945.
[5] A. Lakhan, et al., Mobile-fog-cloud Assisted Deep Reinforcement Learning and Blockchain-enable IoMT System for Healthcare Workflows, Transactions on Emerging Telecommunications Technologies, 2021, p. e4363.
[6] S. Mainali, M.E. Darsie, K.S. Smetana, Machine learning in action: stroke diagnosis and outcome prediction, Front. Neurol. 12 (2021).
[7] Z. Angehrn, et al., Artificial intelligence and machine learning applied at the point of care, Front. Pharmacol. (2020) 11.
[8] S. Wang, et al., Cerebral micro-bleeding detection based on densely connected neural network, Front. Neurosci. 13 (2019) 422.
[9] H.S. Greenwald, C.K. Oertel, Future directions in machine learning, Frontiers in Robotics and AI 3 (2017).
[10] M. Katsuki, et al., Postsurgical functional outcome prediction model using deep learning framework (Prediction One, Sony Network Communications Inc.) for hypertensive intracerebral hemorrhage, Surg. Neurol. Int. 12 (2021).
[11] S. Wang, et al., Cerebral micro-bleed detection based on the convolution neural network with rank based average pooling, IEEE Access 5 (2017) 16576–16583.

[12] P.P. Kim, et al., Cerebral microhemorrhage: a frequent magnetic resonance imaging finding in pediatric patients after cardiopulmonary bypass, Journal of Clinical Imaging Science 7 (2017).
[13] S. Roy, et al., Cerebral microbleed segmentation from susceptibility weighted images, in: Medical Imaging 2015: Image Processing, International Society for Optics and Photonics, 2015.
[14] A.A. Mutlag, M.K.A. Ghani, M.A. Mohammed, A healthcare resource management optimization framework for ECG biomedical sensors, in: Efficient Data Handling for Massive Internet of Medical Things, Springer, 2021, pp. 229–244.
[15] I. Ahmed, E. Balestrieri, F. Lamonaca, IoMT-based biomedical measurement systems for healthcare monitoring: a review, Acta IMEKO 10 (2) (2021) 174–184.
[16] Q. Dou, et al., Automatic detection of cerebral microbleeds from MR images via 3D convolutional neural networks, IEEE Trans. Med. Imag. 35 (5) (2016) 1182–1195.
[17] V. Sundaresan, et al., Automated detection of candidate subjects with cerebral microbleeds using machine learning, Front. Neuroinf. 15 (2022) 80.
[18] S.M. Greenberg, et al., Cerebral microbleeds: a guide to detection and interpretation, Lancet Neurol. 8 (2) (2009) 165–174.
[19] A. Charidimou, D.J. Werring, Cerebral microbleeds: detection, mechanisms and clinical challenges, Future Neurol. 6 (5) (2011) 587–611.
[20] M. Vernooij, et al., Prevalence and risk factors of cerebral microbleeds: the Rotterdam Scan Study, Neurology 70 (14) (2008) 1208–1214.
[21] M.M. Poels, et al., Cerebral microbleeds are associated with worse cognitive function: the Rotterdam Scan Study, Neurology 78 (5) (2012) 326–333.
[22] M.A. Al-Masni, et al., Automated detection of cerebral microbleeds in MR images: a two-stage deep learning approach, Neuroimage: Clinical 28 (2020), 102464.
[23] S. Lu, K. Xia, S.-H. Wang, Diagnosis of cerebral microbleed via VGG and extreme learning machine trained by Gaussian map bat algorithm, J. Ambient Intell. Hum. Comput. (2020) 1–12.
[24] Z. Guo, et al., Robust Spammer Detection Using Collaborative Neural Network in Internet of Thing Applications, IEEE Internet of Things Journal, 2020.
[25] J. Hong, Z. Lu, Cerebral microbleeds detection via discrete wavelet transform and back propagation neural network, in: 2nd International Conference on Social Science, Public Health and Education (SSPHE 2018, 2019 (Atlantis Press).
[26] J. Hong, et al., Detecting cerebral microbleeds with transfer learning, Mach. Vis. Appl. 30 (7–8) (2019) 1123–1133.
[27] L. Zhen, et al., Energy-Efficient Random Access for LEO Satellite-Assisted 6G Internet of Remote Things, IEEE Internet of Things Journal, 2020.
[28] X. Zhang, L. Yang, Z. Ding, J. Song, Y. Zhai, D. Zhang, Sparse vector coding-based multi-carrier NOMA for in-home health networks, IEEE J. Sel. Area. Commun. 39 (2) (Feb. 2021) 325–337, https://doi.org/10.1109/JSAC.2020.3020679.
[29] S. Gregoire, et al., The Microbleed Anatomical Rating Scale (MARS): reliability of a tool to map brain microbleeds, Neurology 73 (21) (2009) 1759–1766.
[30] S.R. Barnes, et al., Semiautomated detection of cerebral microbleeds in magnetic resonance images, Magn. Reson. Imag. 29 (6) (2011) 844–852.
[31] W. Bian, et al., Computer-aided detection of radiation-induced cerebral microbleeds on susceptibility-weighted MR images, Neuroimage: clinical 2 (2013) 282–290.
[32] A. Fazlollahi, et al., Efficient machine learning framework for computer-aided detection of cerebral microbleeds using the radon transform, in: 2014 IEEE 11th International Symposium on Biomedical Imaging (ISBI), IEEE, 2014.
[33] T. Van den Heuvel, et al., Automated detection of cerebral microbleeds in patients with traumatic brain injury, Neuroimage: Clinical 12 (2016) 241–251.
[34] S. Liu, et al., Cerebral microbleed detection using susceptibility weighted imaging and deep learning, Neuroimage 198 (2019) 271–282.
[35] M.A. Mohammed, et al., Novel crow swarm optimization algorithm and selection approach for optimal deep learning COVID-19 diagnostic model, Comput. Intell. Neurosci. (2022) 2022.
[36] A. Suwalska, , et al.Cmb-Hunt, Automatic detection of cerebral microbleeds using a deep neural network, Comput. Biol. Med. 151 (2022), 106233.
[37] J.-H. Kim, et al., Cerebral microbleeds detection using a 3D feature fused region proposal network with hard sample prototype learning, in: International Conference on Medical Image Computing and Computer-Assisted Intervention, Springer, 2022.
[38] Y.-D. Zhang, et al., Seven-layer deep neural network based on sparse autoencoder for voxelwise detection of cerebral microbleed, Multimed. Tool. Appl. 77 (9) (2018) 10521–10538.
[39] H. Chen, et al., Automatic detection of cerebral microbleeds via deep learning based 3D feature representation, in: 2015 IEEE 12th International Symposium on Biomedical Imaging (ISBI), IEEE, 2015.
[40] V. Sundaresan, et al., Automated Detection of Cerebral Microbleeds on MR Images Using Knowledge Distillation Framework, medRxiv, 2021.
[41] Y.-D. Zhang, et al., Sparse Autoencoder based deep neural network for voxelwise detection of cerebral microbleed, in: 2016 IEEE 22nd International Conference on Parallel and Distributed Systems (ICPADS), IEEE, 2016.
[42] S.-Y. Lu, et al., A cerebral microbleed diagnosis method via FeatureNet and ensembled randomized neural networks, Appl. Soft Comput. 109 (2021), 107567.
[43] J. Hong, et al., Classification of cerebral microbleeds based on fully-optimized convolutional neural network, Multimed. Tool. Appl. 79 (21) (2020) 15151–15169.
[44] Y. Tao, R.S. Cloutie, Voxelwise detection of cerebral microbleed in CADASIL patients by genetic algorithm and back propagation neural network, in: 2018 3rd International Conference on Communications, Information Management and Network Security (CIMNS 2018), Atlantis Press, 2018.
[45] H.-n. Wang, B. Gagnon, Cerebral microbleed detection by wavelet entropy and naive Bayes classifier, in: 2nd International Conference on Biomedical and Biological Engineering 2017 (BBE 2017), Atlantis Press, 2017.
[46] Y.-D. Zhang, et al., Cat swarm optimization applied to alcohol use disorder identification, Multimed. Tool. Appl. 77 (17) (2018) 22875–22896.
[47] T. Ateeq, et al., Ensemble-classifiers-assisted detection of cerebral microbleeds in brain MRI, Comput. Electr. Eng. 69 (2018) 768–781.
[48] M.A. Al-Masni, et al., A two cascaded network integrating regional-based YOLO and 3D-CNN for cerebral microbleeds detection, in: 2020 42nd Annual International Conference of the IEEE Engineering in Medicine & Biology Society (EMBC), IEEE, 2020.
[49] Q. Dou, et al., Automatic cerebral microbleeds detection from MR images via independent subspace analysis based hierarchical features, in: 2015 37th Annual International Conference of the IEEE Engineering in Medicine and Biology Society (EMBC), IEEE, 2015.
[50] S. Lu, et al., Detection of cerebral microbleeding based on deep convolutional neural network, in: 2017 *14th* International Computer Conference on Wavelet Active Media Technology and Information Processing (ICCWAMTIP), IEEE, 2017.
[51] P. Doke, et al., Using CNN with Bayesian optimization to identify cerebral micro-bleeds, Mach. Vis. Appl. 31 (5) (2020) 36.
[52] J. Hong, et al., Improvement of cerebral microbleeds detection based on discriminative feature learning, Fundam. Inf. 168 (2–4) (2019) 231–248.
[53] S. Sa-ngiem, et al., Cerebral microbleed detection by extracting area and number from susceptibility weighted imagery using convolutional neural network, in: Journal of Physics: Conference Series, IOP Publishing, 2019.
[54] H. Liu, et al., Adaptive squeeze-and-shrink image denoising for improving deep detection of cerebral microbleeds, in: Medical Image Computing and Computer Assisted Intervention–MICCAI 2021: 24th International Conference, Strasbourg, France, September 27–October 1, 2021, Proceedings, Part VI 24, Springer, 2021.
[55] J.-H. Kim, et al., A single-stage detector of cerebral microbleeds using 3D feature fused region proposal network (FFRP-Net), in: 2022 IEEE 4th International Conference on Artificial Intelligence Circuits and Systems (AICAS), IEEE, 2022.
[56] Z. Wei, et al., Construction of a medical micro-object cascade network for automated segmentation of cerebral microbleeds in susceptibility weighted imaging, Front. Bioeng. Biotechnol. 10 (2022), 937314.
[57] H. Lee, et al., Detection of cerebral microbleeds in MR images using a single-stage triplanar ensemble detection network (TPE-Det), J. Magn. Reson. Imag. 58 (1) (2023) 272–283.
[58] S. Wang, et al., Cerebral micro-bleeding identification based on a nine-layer convolutional neural network with stochastic pooling, Concurrency Comput. Pract. Ex. 32 (1) (2020) e5130.
[59] M.L. Seghier, et al., Microbleed detection using automated segmentation (MIDAS): a new method applicable to standard clinical MR images, PLoS One 6 (3) (2011).
[60] B. Ghafaryasl, et al., A computer aided detection system for cerebral microbleeds in brain MRI, in: 2012 9th IEEE International Symposium on Biomedical Imaging (ISBI), IEEE, 2012.

[61] X. Zou, et al., Automated algorithm for counting microbleeds in patients with familial cerebral cavernous malformations, Neuroradiology 59 (7) (2017) 685–690.
[62] S.P. Singh, et al., 3D Deep Learning on Medical Images: A Review, 2020 arXiv preprint arXiv:2004.00218.
[63] F.S. Feltrin, et al., Longitudinal changes in brain volumetry and cognitive functions after moderate and severe diffuse axonal injury, Brain Inj. 32 (11) (2018) 1413–1422.
[64] A.A. Gouw, et al., Heterogeneity of small vessel disease: a systematic review of MRI and histopathology correlations, J. Neurol. Neurosurg. Psychiatr. 82 (2) (2011) 126–135.
[65] B. Psaila, et al., Intracranial hemorrhage (ICH) in children with immune thrombocytopenia (ITP): study of 40 cases, Blood, The Journal of the American Society of Hematology 114 (23) (2009) 4777–4783.
[66] H.-C. Koennecke, Cerebral microbleeds on MRI: prevalence, associations, and potential clinical implications, Neurology 66 (2) (2006) 165–171.